JAAS

Accepted Manuscript

This article can be cited before page numbers have been issued, to do this please use: T. Rodríguez, S. P. Limandri, S. Suárez, I. Ortega-Feliu and J. C. Trincavelli, *J. Anal. At. Spectrom.*, 2017, DOI: 10.1039/C7JA00068E.

ROYAL SOCIETY OF CHEMISTRY

rsc.li/jaas

View Article Online
DOI: 10.1039/C7JA00052F

Journal Name

ARTICLE TYPE

Cite this: DOI: 10.1039/xxxxxxxxxx

Received Date
Accepted Date

DOI: 10.1039/xxxxxxxxxx

www.rsc.org/journalname

Standardless semi-quantitative analysis by PIXE

T. Rodríguez,[a,b] S. Limandri,[a,b] S. Suárez,[c] Inés Ortega-Feliu,[d] J. Trincavelli,[a,b]‡

A method based on the refinement of atomic and experimental parameters developed for the description of PIXE spectra is presented and applied to standardless semi-quantitative PIXE analysis. This method was implemented in the sofware PAMPA (Parameter Assessment Method for PIXE Analysis) and consists in minimizing the quadratic differences between an experimental spectrum and an analytical function proposed to describe it. The first results of PAMPA are presented for the quantification of synthetic and mineral, thin and bulk samples, and they were compared with results obtained with a commercial software.

1 Introduction

Particle induced x-ray emission (PIXE) is a powerful non-destructive analytical technique used in different fields of science and industry. One of the main advantages of this technique is its very low detection limit, which allows for trace element characterization.

In PIXE, like in some other spectroscopical techniques, the input information is an x-ray spectrum and the output result is a set of mass concentrations. Thus, to obtain reliable concentrations, the main conditions that need to be fulfilled for the input data: the spectrum must have an energy resolution good enough to discriminate the different peaks involved, and each of these peaks must have a number of counts leading to statistically significant results. The procedure to obtain the output information from the input data, *i.e.*, the mass concentrations from the spectrum, can be a hard task (even for high quality spectra) that comprises several steps in which all the concentrations and other atomic and instrumental parameters are related among themselves in a complex way.

This work introduces a method to fit the experimental PIXE spectrum by means of an analytical function whose fitting parameters can be chosen by the user. The whole set of optimizable magnitudes involves instrumental parameters, scale factors, atomical parameters and the mass concentrations. This method was implemented in a software called "Parameter Assessment Method for PIXE Analysis" (PAMPA), which is available on internet[1]. A software analog to PAMPA for electron probe microanalysis was published before[2] and several parallel considerations can be done. Both programs allows for different tasks depending on which parameters are set as known and which ones are optimized. For instance, if the sample is perfectly known and the atomic parameters involved are known with sufficient precission, instrumental parameters, such as those associated with detection efficiency[2] or peak asymmetry (related to incomplete charge collection in the detector)[3] can be assessed. On the other hand, once the detection system has been properly characterized, different atomic parameters can be obtained, such as characteristic energies[4], relative transition probabilities[5], natural linewidths[6], or parameters related to satellite lines[7,8]. Finally, if everything else is known with sufficient accuracy, the mass concentrations can be set as the refinable parameters of the fitting process. In the latter case, the software becomes a quantification tool or, at least, allows for semi-quantitative standardless assessments[9]. This situation is faced in the present work for proton incidence.

Three kinds of samples can be analyzed by PIXE: thick, thin and intermediate samples. When samples are thick enough to completely stop the particle beam, there is no need to know the sample thickness to carry out quantification, since the integrals involved in the quantification procedures are computed for thick-

[a] *Instituto de Física Enrique Gaviola, Ciudad Universitaria, 5000, Córdoba, República Argentina*
[b] *Facultad de Matemática, Astronomía y Física, Universidad Nacional de Córdoba, Ciudad Universitaria, 5000, Córdoba, República Argentina*
[c] *Instituto Balseiro, Universidad Nacional de Cuyo, Bustillo 9500, San Carlos de Bariloche, Río Negro, Argentina*
[d] *Centro Nacional de Aceleradores (Universidad de Sevilla-CSIC-Junta de Andalucía), Avda. Thomas A. Edison 7, Seville, Spain*
‡ E-mail: trincavelli@famaf.unc.edu.ar.

View Article Online
DOI: 10.1039/C7JA00068E

nesses from zero to infinity. This "infinity" thickness, in practice can be reached at 100 μm. On the other hand, when the sample is very thin, the absorption of x-rays within the sample in their way to the detector can be neglected, and all the calculations are simplified. Nevertheless, in the latter case the sample thickness is required, and its value can be obtained iteratively during the quantification procedure, along with the concentrations. Finally, for the analysis of intermediate samples, the integral must be carried out up to the proton exit energy or up to the sample thickness, depending on which of them is known.

Several quantification procedures have been developed and implemented for different kinds of samples in software for obtaining the elemental composition by PIXE, for example, GUPIX[10–13], GeoPIXE[14], TTPIXAN[15], PIXYKLM[16], PIXEF[17], and SAPIX[18]. Some of these software tools were developed and optimized only for local use, whereas other ones are more versatile packages and were open to the users community. The performance of some of them for peak deconvolution and background subtraction was faced in an intercomparison study organized by the International Atomic Energy Agency[19,20]. From this study, it was concluded that most of the programs obtain peak areas reasonably well. Nevertheless, even when a precise determination of peak areas is one of the most important quantification steps, some effects related to the emitted x-rays, *i.e.*, production, absorption and detection, must also be carefully taken into account to obtain mass concentrations from peak areas. The level of accuracy at which these processes are known has a direct impact on the quantification results.

Basically, all the quantification software tools available for PIXE work in the following way: first, the selected peak areas are obtained from a non-linear least squares minimization procedure. To this purpose, the background must be previously subtracted and certain peak profiles must be fitted to the remaining spectrum. Regarding the background subtraction, different approaches have been followed, such as the application of mathematical filters to the whole spectrum, or the use of empirical or semiempirical background models. For the line shapes, Hypermet functions are the most used profiles because they account for Gaussian instrumental broadening and peak tailing at the low energy side, related to incomplete charge collection in the detector. In addition, step functions are also used to consider absorption effects. The parameter to minimize in order to get a good fit is the so called χ^2; it represents the quadratic difference between the experimental and the calculated spectrum, weighed by a statistical factor, which is usually the inverse of the square root of the number of experimental counts. The peak areas obtained by the fitting process are then corrected by absorption (when filters are used to prevent detector saturation) and detection effects (pile-up and detector efficiency). Finally, the comparison of these corrected areas to the calculated x-ray yields leads to a set of concentrations. In this process, a peak (or multiplet) is assigned to each element to be quantified.

The most versatile and used quantification software packages are GeoPIXE and GUPIX. The first one was optimized for its application in the field of geoscience and was extended for map acquisition and quantification by microPIXE[21–24]. The second one has been used to study different kinds of materials[25–28], and from its creation, different modifications were performed, which are related to the user interface[11–13], the physical parameter databases[12,14], and the detection efficiency correction procedures[14]. The main characteristics of the software packages mentioned in this section are very concisely presented in table 1; for a more detailed description see refs.[10–20,29].

In this work, the main characteristics of PAMPA software package are presented and its performance is tested when used as a quantification routine; to this purpose, mass concentrations obtained by PAMPA are compared to the ones obtained with GUPIX[12] for several thin and thick samples.

2 Experimental

Proton induced x-ray spectra from thin film samples deposited on 2.5 μm mylar substrates were measured with the NEC 3 MV Tandem accelerator available at the Centro Nacional de Aceleradores, Sevilla, Spain. The samples analyzed were: CaF_2, NaCl, CsBr, RbI, KCl, BaF_2 and GdF_3, all of them supplied by Micromatter Co., with a nominal 50 $\mu g/cm^2$ thickness certified to $\pm$ 5%. All the spectra were induced by 3 MeV proton beams, collecting a total charge between 0.5 and 1 μC, except for BaF_2, where 5 MeV protons were used and the collected charge was 2 μC. The Si(Li) SSL30150 detector used has a 8-μm-thick Be window, a 3-mm-thick active layer, a 0.1-μm-thick dead layer, a 70-nm-thick Al electric contact and an active area of 30 mm^2, according to the manufacturer. This detector was positioned at 18 mm from the sample surface, and the x-rays were collected at a 45° take-off angle.

On the other hand, spectra from thick samples were obtained at the 1.7 MV Tandem accelerator of the Centro Atómico Bariloche, Argentina. The thick samples studied were: MgO (#1), muscovite (#2), feldspar (#3), kaolinite (#4), NbO_2 (#5), Fe_2O_3 99%-Al_2O_3 1% (#6), CoO 5%-Cr_2O_3 95% (#7), BCR (Basalt, Columbia River) (#8) and GSP (Granodiorite, Silver Plume) (#9). Spectra were induced by 2 MeV proton beams, collecting a total charge of 1 μC for each spectrum. The x-ray detector used was an SDD e2v SiriusSD with ultrathin polymer window, with a 30 mm^2 nominal area placed at 15 cm from the sample (solid angle of 1.33 10^{-3} srad). According to the data provided by the manufacturer, the ultrathin window Moxtek AP3.3 has a 380-μm-thick silicon support structure with a 77% open area and a 300 nm polymer layer. The detector has an aluminum electric contact (30 nm thick) and an active thickness of 0.045 cm.

View Article Online
DOI: 10.1039/C7JA00068E

Table 1 Main features of several PIXE quantification routines.

	GeoPIXE	GUPIX	PIXAN/ TTPIXAN	PIXYKLM	PIXEF	SAPIX
Sample	Thin, interm., thick, stratified	Thin, interm., thick, stratified	Thin, thick	Thin, thick	Thick	Thin, thick
Developer	CSIRO Australia	Guelph Univ. Canada	ANSTO Australia	ATOMKI Hungary	LLNL USA	NMCC Japan
K lines	6≤Z≤92	6≤Z≤92	5≤Z≤62	5≤Z≤56	11≤Z≤56	10≤Z≤60
L lines	20≤Z≤92	22≤Z≤92	40≤Z≤92	17≤Z≤92	32≤Z≤94	30≤Z≤90
M lines	73≤Z≤92	72≤Z≤83, 90-92	No	31≤Z≤92	No for quant.	No
Incident particles	^{1}H,^{4}He: 2-5 MeV	^{1}H ≤5 MeV ^{2}H ≤6 MeV ^{3}He ≤12 MeV ^{4}He ≤12 MeV ^{1}H 20-80 MeV	^{1}H	In principle, ions of any Z and energy	^{1}H	^{1}H, ^{2}H, ^{3}He, ^{4}He 0.1-40 MeV
Back-ground	• SNIP • User defined	Top-hat filter	• EXP + absorption • Iterative	• EXP + absorption • Iterative • Experimental	• SNIP • Clayton's method	• EXP • User defined
Peak shape	Gaussian + EXP tail + Stefan-Boltz.	Voigt + EXP tail + flat step	Gaussian + EXP tail + step	• Gaussian • Voigt + EXP tail	• Gaussian + EXP tail • Hypermet	• Response function • Gaussian

Thick samples were prepared from powder analytical grade reagents (except for the certified powder standards #8 and #9); particularly, samples #6 and #7 were made by weighting and mixing different compounds. Samples # 1 to #7 were analized by Wavelength Dispersive X-Ray Fluorescence (WD-XRF). For the analysis of sample #1, an F8 Tiger (Bruker) spectrometer was used, while a Magi'X (PANanalytical) spectrometer was used for samples #2 to #7. For the analysis performed with both spectrometers, the excitation was carried out by means of a Rh anode and the detection was performed in He atmosphere. With the aim of achieving a lower XRF detection limit, the corresponding seven samples were fused to form glass discs in a Claisse M4 gas fluxer using a $LiBO_2$ 50%-$Li_2B_4O_7$ 50% mixture as a flux. For this reason, taking into account that some material can be lost in the fusion process, the powder samples were calcinated at a similar temperature (around 700 °C) before preparing the pellets to be analyzed by PIXE. In the case of samples #8 and #9, the nominal certified composition (certified by U.S. Geological Survey Geochemical Reference Materials and Certificates) was taken for comparison. To obtain the nine pellets, the powders were deposited in aluminum 6 mm-diameter cups and compressed with a hydraulic press.

3 Spectral Analysis

The spectral processing carried out is based in a method of parameter optimization, which consists in minimizing the function

$$\chi^2 = \frac{1}{N-P}\sum_i \frac{(\bar{I}_i - I_i)^2}{\bar{I}_i}. \quad (1)$$

This function represents the squared differences between an experimental x-ray spectrum $\bar{I}_i$ and an analitycal function I_i proposed to describe it[2], which depends on atomic and experimental parameters and takes into account the continuous background, the characteristic peaks from the elements present in the sample, and the spurious peaks, such as sum peaks and the Si internal fluorescence peak. The sum in Eq. (1) runs over all the spectrum channels and the function I_i is given by

$$I_i = B(E_i) + \sum_{j,q} P_{j,q} H_{j,q}(E_i) + \sum_{sp,i} I_{sp} H_{sp}(E_i), \quad (2)$$

where B is the measured continuum background, H is the profile for the detected characteristic lines, and P denotes their intensity, the subindices j and q represent the corresponding element and line, I_{sp} and H_{sp} are, respectively, the intensity and profile of each of the spurious peaks, and E_i is the energy of channel i.

View Article Online
DOI: 10.1039/C7JA00068E

3.1 Minimization procedure

The algebraic complexity of the expression for χ^2 involving the predicted intensity I_i for every channel requires a numerical procedure for its minimization. The downhill simplex algorithm[30] was chosen for the present application because it is a robust routine, and requires only function evaluations, not derivatives. This fact is particularly important since it is often necessary to deal with functions whose computed derivatives do not accurately point the way to the minimum, usually because of truncation error in the method of derivative evaluation.

Along with the simplex algorithm, a penalty function was implemented in the cases for which a constrain is needed to be imposed. That is the case, for instance, of mass concentrations, which are restricted to positive or null values. In this case, the function χ^2 to be minimized is modified so that it takes a large positive value for negative values of the constrained parameters. Thus, the new function to be minimized can be defined as

$$F(\{x_k\}) = \chi^2(\{x_k\}) + p(\{x_k\}), \tag{3}$$

where the penalty function p, depending on the optimized parameters $\{x_k\}$ takes large positive values when the constrain is not fulfilled and it is zero in the other case. In the particular case of mass concentrations:

$$p(\{x_k\}) = L \sum_{j=1}^{N} \min\{0, x_j\}. \tag{4}$$

In the described example, the N mass concentrations are denoted as x_j parameters, which are included in the set of optimized $\{x_k\}$ parameters; the constant L is a large negative number.

3.2 Characteristic peaks

For thin samples the detected characteristic intensity $P_{j,q}$ of the line q corresponding to a decay to an ℓ shell of the element j, can be expressed as[31]

$$P_{j,q} = \frac{\beta N_{av} \sigma_{j,\ell}(E_0) \omega_{j,\ell} b_{j,q} \varepsilon(E_{j,q}) \left(\frac{\Omega}{4\pi}\right) C_j \rho t}{A_j \cos\alpha}, \tag{5}$$

where β is a constant proportional to the number of protons, N_{av} is Avogadro's number, $\sigma_{j,\ell}$ is the ℓ-shell final vacancy production cross section of element j, $\omega_{j,\ell}$ is the corresponding fluorescence yield, E_0 is the energy of the primary beam, $b_{j,q}$ is the q-line relative transition probability, $\varepsilon(E_{j,q})$ is the detection efficiency at the characteristic line of interest, $\Omega/4\pi$ is the solid angle fraction subtended by the detector, C_j is the mass concentration of element j, ρt is the mass thickness, A_j is the atomic mass of element j and α is the proton impact angle with respect to the direction normal to the sample surface.

In the case of transitions to L shells, the final vacancy production cross-sections are related to the ionization cross sections σ_ℓ by

$$\sigma_{L_1} = \tilde{\sigma}_{L_1} \tag{6}$$

$$\sigma_{L_2} = \tilde{\sigma}_{L_2} + f_{12}\tilde{\sigma}_{L_1} \tag{7}$$

$$\sigma_{L_3} = \tilde{\sigma}_{L_3} + f_{23}\tilde{\sigma}_{L_2} + (f_{13} + f_{12}f_{23})\tilde{\sigma}_{L_1}\,, \tag{8}$$

where f_{kj} is the probability of a Coster-Kronig transition from an initial state with a vacancy in the L_k subshell to a final state with a vacancy in the L_j subshell.

For thick and homogeneous samples, the detected characteristic intensity can be expressed as[31]

$$P_{j,q} = \frac{\beta N_{av} \omega_{j,\ell} b_{j,q} \varepsilon(E_{j,q}) \left(\frac{\Omega}{4\pi}\right) C_j}{A_j \cos\alpha} \int_{E_0}^{0} \frac{\sigma_{j,\ell}(E) T_{j,q}(E) dE}{S(E)}, \tag{9}$$

where $S = -dE/d\rho z$ is the stopping power (ρz being the mass thickness variable) and $T_{j,q}$ is the photon attenuation given by

$$T_{j,q} = \exp\left\{ -\left(\frac{\mu}{\rho}\right)_{j,q} \frac{\cos\alpha}{\sin\theta_{toff}} \int_{E_0}^{E} \frac{dE}{S(E)} \right\}, \tag{10}$$

where $(\mu/\rho)_{j,q}$ is the mass attenuation coefficient for the characteristic line of interest and θ_{toff} is the angle between the sample surface and the detector.

3.3 Continuum background

A semi-empirical model is used to predict the continuum background B_g generated in the sample[32], given by

$$\log(B_g(E)/d) = a + cE, \tag{11}$$

where a, c and d are constants and E is the photon energy. This model was developed to predict the continuous background generated in a carbon sample, but its functional shape also describes properly the background produced by other materials.

In order to obtain the emitted background B_e the model must be corrected for photon attenuation in the sample. For a thin layer placed at a mass thickness ρz, B_e can be related to B_g by

$$B_e = \exp[-(\mu/\rho)(\rho z)\mathrm{cosec}(\theta_{toff})] B_g. \tag{12}$$

For thick samples, the emitted background can be obtained by integration of Eq.(12) from $\rho z = 0$ to the maximum penetration depth of protons ρz_{max} in the sample. By assumming a step model for B_g, it is possible to easily calculate the integral, and the emitted bremsstrahlung is

$$B_e = \frac{1 - \exp[-(\mu/\rho)(\rho z_{max})\mathrm{cosec}(\theta_{toff})]}{\mu\,\mathrm{cosec}(\theta_{toff})} B_g, \tag{13}$$

View Article Online
DOI: 10.1039/C7JA00068E

where ρz_{max} is obtained from the sample stopping power, which depends on all the mass concentrations.

3.4 Peak shape

Any characteristic line q of an element j registered by a Si(Li) or an SD detector can be roughly described by a Gaussian profile $G_{j,q}(E_i)$ of width $\sigma_{j,q}$ given by

$$\sigma_{j,q} = \sqrt{n^2 + \varepsilon_0 F E_i}, \tag{14}$$

where n is related to the electronic noise associated with the amplification process, F is the Fano factor, which is related to fluctuations in the electric charge collected by the detector, ε_0 is the energy required to create an ion-electron pair in the detector crystal and E_i is the photon energy.

A more careful description must take into account the asymmetric tail at the low energy side of the peak due to incomplete charge collection. The peak profile used in PAMPA accounts for this effect by means of an exponential tail convoluted with a Gaussian function[3]. The asymmetric shape is characterized by two parameters: the amplitude $t_{j,q}$ and the width $\beta_{j,q}$, and it is given by

$$Q_{j,q}(E_i) = \frac{1}{2} t_{j,q} \exp \frac{\sigma_{j,q}^2}{2\beta_{j,q}^2} \exp \frac{(E_i - E_{j,q})}{\beta_{j,q}} \cdot \operatorname{erfc}\left(\frac{E_i - E_{j,q}}{\sqrt{2}\sigma_{j,q}} + \frac{\sigma_{j,q}}{\sqrt{2}\beta_{j,q}} \right) \tag{15}$$

Thus, the characteristic peak profile can be expressed as

$$H_{j,q}(E_i) = M(G_{j,q}(E_i) + Q_{j,q}(E_i)), \tag{16}$$

where M is a normalization factor defined so that the integral of $H_{j,q}(E_i)$ be equal to one.

3.5 Efficiency

In order to determine the detector efficiency, for both detectors used here (Si(Li) and SDD), it must be born in mind that to actually count a photon, it must arrive to the detector active region passing through a supporting grid (only present in the SDD used) and several layers: the window, the metallic ohmic contact and the so-called dead layer, where detection is not possible. Taking into account the different layers of the detector, the intrinsic efficiency $\varepsilon_{\text{O.A.}}$ of the detector open area, *i.e.*, the detector region not hidden behind the silicon supporting grid, is given by:

$$\varepsilon_{\text{O.A.}} = e^{-(\mu/\rho\ \rho x)_{\text{win}}} e^{-(\mu/\rho\ \rho x)_{\text{Al}}} e^{-(\mu/\rho\ \rho x)_{\text{DL}}} \left[1 - e^{-(\mu/\rho\ \rho x)_{\text{det}}}\right], \tag{17}$$

where $(\mu/\rho\ \rho x)_i$ is the product of the mass absorption coefficient, the mass density and the thickness of the i-th detector layer. The first factor is related to the attenuation of the incident photons in the detector window, the second one accounts for the photon losses in the aluminium ohmic contact, the third one takes into account the absorption in the dead layer and the last one is the probability that a photon be absorbed in the detector active region.

The Si(Li) detector used for the analysis of thin samples lacks of a supporting grid, thus, the expression given in Eq.(17) represents the intrinsic efficiency. In the case of the SD detector, instead a silicon grid that acts as a supporting structure for the window must be taken into account. Considering this fact, the following expression is obtained for the intrinsic efficiency:

$$\varepsilon = 0.77\, \varepsilon_{\text{O.A.}} + 0.23\, \varepsilon_{\text{O.A.}} e^{-(\mu/\rho)_{\text{Si}} \rho_{\text{Si}} x_{\text{grid}}}, \tag{18}$$

where x_{grid} is the supporting grid thickness, $(\mu/\rho)_{\text{Si}}$ and ρ_{Si} are the mass absorption coefficient and density of the grid material (silicon in this case), respectively. The first term of Eq.(18) takes into account the arrival of photons to the detector open area, which represents a 77% of the total detector area, whereas the second one accounts for the fraction that previously passed through the grid.

The efficiency of an energy dispersive spectrometer is very sensitive to the thickness values involved in Eq.(17), which usually are known with low accuracy because of uncertainties related to the manufacturing process and also due to variations in the original values produced over time. These modifications can arise from window contamination and from changes in the dead layer. In order to face this problem, the nominal thickness values of the Si(Li) detector, used in this work for the quantification of thin samples, were recalculated. These thicknesses were obtained by using Eq.(17) and imposing that quantification performed with both softwares (GUPIX and PAMPA) leads to the nominal mass concentrations for each sample. The mean values of each parameter were calculated producing two thickness sets: one for each software. The thicknesses obtained with each software are shown in Table 2 along with the nominal values. The active layer was kept fixed as its nominal value of 3 mm, because this is a more reliable parameter than the other thicknesses and it is not expected to change over time.

Table 2 Characteristic thicknesses obtained for the Si(Li) detector used.

	Nominal	GUPIX	PAMPA
Be window (μm)	8	16.0	12.9
Al contact (nm)	70	10	10
Dead layer (μm)	0.1	0.18	0.39

Regarding the detector efficiency of the SDD used for the analysis of thick samples, it was previously studied for energies between 0.27 and 25 keV[33] by comparing experimental

View Article Online
DOI: 10.1039/C7JA00068E

intensities produced under 2-MeV proton impact on samples of known stoichiometry, with values of the involved x-ray yields. The intrinsic efficiency values at different energies obtained in that article were used for the quantification performed here using both software packages. It must be emphazised that this efficiency determination was based on x-ray yields calculated using the GUYLS software included in GUPIX package, thus, it was optimized for the quantification models implemented in this software.

3.6 Databases

Several parameters can be optimized by PAMPA; some are related to instrumental magnitudes like the *zero* and *gain* calibration parameters, the noise n and Fano factor F involved in peak broadening, the amplitude $t_{j,k}$ and width $\beta_{j,k}$ related to peak asymmetry, and the thicknesses characteristic of the detector window. Other refinable parameters are the three constants needed to describe the continuum spectrum and a scale factor for the characteristic peaks; some atomic magnitudes can also be optimized like characteristic energies and relative transition probabilities (RTP). When PAMPA is used as a quantification tool, the optimizable parameters of interest are the mass concentrations and most of the other magnitudes are kept fixed, as explained in the following subsection.

Additional physical magnitudes necessary to peform the calculations implemented in PAMPA to relate the experimental intensities to the searched mass concentrations are not refinable parameters but they were taken from the literature. The K fluorescence yields correspond to data published by Krause[34], whereas for L shell fluorescence yield, values tabulated by Perkins *et al.*[35] are considered. Coster-Kronig transition $f_{2,3}$ probabilities were taken from the values recommended by Krause[34] for $28<Z<35$, while for $36<Z<92$ the values recommended by Campbell were used[36]. Regarding $f_{1,2}$ and $f_{1,3}$, for $22<Z<24$, the data published by McGuire were used[37]; for $f_{1,2}$ in the range $25<Z<59$, the values calculated by Campbell in the Dirac-Hartree-Slater approximation were considered, while the values recommended by this author were used for higher atomic number elements[36]. Finally, for $f_{1,3}$ data recommended by Krause for $25<Z<38$ and by Campbell for the remainder elements were used. Regarding K- and L-x-ray production cross sections, results obtained from the theoretical ECPSSR model (Energy-Loss Coulomb-Repulsion-Perturbed Stationary State Relativistic) by Brandt and Lapicki[38] are used from the data base available in the software package Geant4[39]. Stopping power values for each element are assessed by means of SRIM sofware (Stopping and Range of Ions in Matter)[40]. The mean stopping power of the sample is assessed using the Bragg's rule. Finally, mass atenuation coefficients are calculated with the model proposed by Heinrich[41].

3.7 Software specifications and fitting methodology

The software package PAMPA was written in Object Pascal; it runs under Linux (Ubuntu) or Windows operative systems. The menu environment was developed with the open-source cross platform IDE Lazarus and the graphical output is generated with the Gnu-Plot function and data plotting program. Figure 1 shows some of the menus available.

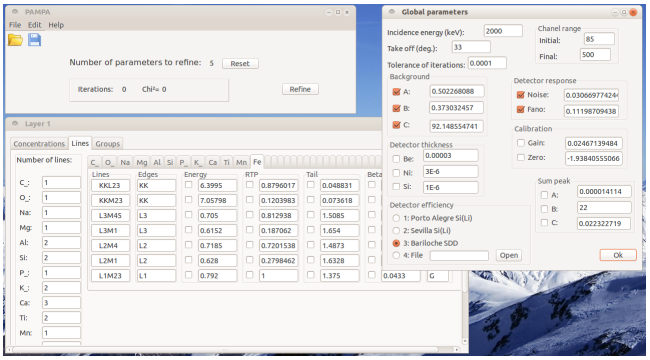

Fig. 1 PAMPA environment. Different menus available.

The analyzable elements range from B to U, including up to 30 elements for analysis. The present version of the program permits to include up to 30 K and L lines for each element in the input file, although an extension to M lines would be straightforward, provided reliable databases are available for x-ray production cross sections.

Regarding the ionization source, PAMPA can be applied to protons in all the energy range of interest in PIXE, since the databases used for both ionization cross section and stopping power are, in principle, available for the very wide range between 10 keV and 10 GeV. An extension to alpha particles would only require the implementation of the corresponding databases.

The software displays the predicted and experimental spectra, in addition to their differences, each time certain pre-established criterion of convergence is fulfilled. Thus, by means of a visual examination of the intermediate results it is possible to make an appropriate decision for the subsequent strategy. For an easy visualization of the spectral output, different colors are assigned to the whole spectrum fitting, the characteristic peaks, the continuous background, sum peaks, asymmetric peak tails and residuals.

All the minimization methods can lead to a local minimum instead of the searched global minimum. To face this problem it is helpful to start from reasonable initial values for the parameters to be optimized. A way to confirm that the minimum found is the global one is by changing the set of initial values used. Usually, it is recommended to carry out the procedure by choosing few parameters at a time; once their values have been achieved, they may be set fixed so that other reduced group of parameters is allowed to vary. When all the chosen parameters are refined,

View Article Online
DOI: 10.1039/C7JA00068E

the procedure may be restarted with the obtained values as initial guesses, varying all of them simultaneously.

For the quantification performed here, the characteristic energies and relative transition probabilities were set as fixed parameters, and their values were taken from the data published by Bearden[42] for characteristic energies, by Scofield[43] for K-line RTPs and by Campbell and Wang[44] for L-line RTPs. On the other hand, the efficiency parameters were determined and kept fixed as detailed in Sec. 3.5.

Regarding the parameters related to peak asymmetry, they were assessed as follows: 1. in a wide region of the spectrum involving all the peaks, the calibration (*zero* and *gain*) and detector response (n and F) parameters were optimized along with the background factors (a, c and d); 2. In a narrow region around each well defined peak, the peak scale factor β together with the electronic noise n were refined keeping fixed the other parameters; 3. The asymmetry parameters $\beta_{j,q}$ and $t_{j,q}$ were added to the refinable parameters in the same narrow region; 4. The values obtained for $\beta_{j,q}$ and $t_{j,q}$ were used to calculate the asymmetric area given by

$$A_{j,q} = \int_{-\infty}^{\infty} MQ_{j,q}(E)dE; \tag{19}$$

5. The values obtained for $A_{j,q}$ and $t_{j,q}$ were fitted as a function of photon energy, averaging values when more than one spectrum was available for the same characteristic energy. The curve corresponding to $A_{j,q}$ is shown in Fig. 2, whereas $t_{j,q}$ exhibits a similar behavior with the characteristic energy. These fitting curves were used to obtain the asymmetry parameters $\beta_{j,q}$ and $t_{j,q}$ of all the peaks involved in the analysis of thick samples (no asymmetric correction was necessary for the analysis of the thin samples, characterized with a different spectrometer). The first parameter was calculated using Eqs.(15) and (19) from the value obtained for $A_{j,q}$, because the latter is more stable than $\beta_{j,q}$[3].

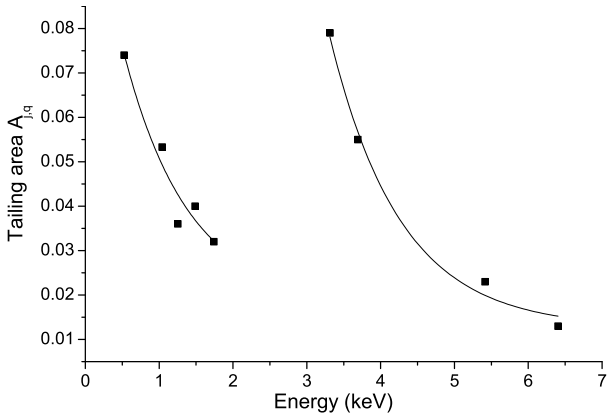

Fig. 2 Values obtained for areas $A_{j,q}$ as a function of characteristic energy.

It is interesting to note the similarity between the energy dependence of the area $A_{j,q}$ and the Si mass absorption coefficient. This fact corroborates that the detector crystal region of highest concentration of trapping sites, which are responsable for incomplete charge collection, is the closest to detector surface, below the dead layer.

Notice that certain tasks, like the characterization of peak shape profiles, or the determination of the detector efficiency, should be performed only for the first analyses carried out with a particular spectrometer, and eventually, the obtained parameters should be updated periodically.

Once the asymmetry parameters were estimated, the procedure for obtaining the mass concentrations was carried out in two steps. Firstly, the parameters n and F related to the peak width, the calibration *zero* and *gain*, the continuum a, c and d constants and the peak scale factor β were refined. The initial guesses for the concentrations were assessed as the ratio between each peak maximum intensity and the sum of all these intensities. When the best spectral fit was obtained, the mass concentrations C_j were added to the set of optmized parameters.

4 Results and discussion

In the present section, the concentrations obtained by means of PAMPA and GUPIX are presented and compared for both thin and thick samples. The results obtained using both methods and the nominal values (or those obtained by XRF analysis) were normalized to unity.

In order to show the discrepancies between the calculated concentrations C_i and the nominal values C_i^n, a parameter ε is defined as a weighted average of the relative errors of all the elements analyzed in the sample, multiplied by 100, the weight factors being the respective concentrations. In this way, the most abundant elements in the sample are considered as the most important contributors of ε. Thus, the parameter ε can be expressed as

$$\varepsilon = \frac{\sum |C_i - C_i^n|}{\sum C_i^n} \times 100\,. \tag{20}$$

The sum in the denominator is a normalization factor close to unity; it runs over all the elements simultaneously present in the reference composition, and in GUPIX and PAMPA quantifications.

Figures 3 and 4 show some examples of spectral fitting with PAMPA for thin and thick samples, respectively. Several cases of overlapped, weak and sum peaks can be seen properly fitted along with the contribution of the continuum background, whose adequate description is necessary to determine the neat peak intensities. The Si internal fluorescence peak can also be seen for the CaF_2 spectrum.

It must be mentioned here that the quantification with GUPIX must be performed choosing particular lines or line groups. Unfortunately the concentration obtained may vary noticeably de-

View Article Online
DOI: 10.1039/C7JA00068E

pending on the selection made. In all the cases when more than one group of lines (K or L) was available, the one which produced the concentrations closer to the nominal values was selected. PAMPA, instead, performs quantification with all the spectrum or, at least, with the spectral region selected by the user.

4.1 Thin samples

Mass concentrations of 14 elements corresponding to 7 different samples deposited on mylar substrates: CaF_2, NaCl, CsBr, RbI, KCl, BaF_2 and GdF_3, were determined. The values obtained are shown in Table 3, where they are also compared with nominal concentrations and with the quantifications performed using GUPIX. For 5 of the 7 thin samples studied, PAMPA produced better results than GUPIX, *i.e.*, from the 14 elements studied, the values obtained with PAMPA are closer to the nominal concentrations for 10 elements, while GUPIX produced closer concentrations in 4 cases.

Table 3 Mass concentrations obtained for thin samples.

Sample	Element	Nominal	GUPIX	PAMPA
CaF_2	F	0.4870	0.5612	0.537
	Ca	0.5130	0.4408	0.463
ε			14.6	10.1
NaCl	Na	0.3934	0.3770	0.373
	Cl	0.6066	0.6300	0.627
ε			4.7	4.0
CsBr	Br	0.3755	0.3777	0.349
	Cs	0.6245	0.6223	0.650
ε			0.4	5.1
RbI	Rb	0.4024	0.4809	0.428
	I	0.5976	0.5191	0.572
ε			15.7	5.1
KCl	Cl	0.4756	0.4781	0.471
	K	0.5244	0.5219	0.526
ε			0.5	0.3
BaF_2	F	0.2170	0.1784	0.195
	Ba	0.7830	0.8216	0.805
ε			7.7	4.4
GdF_3	F	0.2660	0.2285	0.216
	Gd	0.7340	0.7741	0.784
ε			7.8	10.1

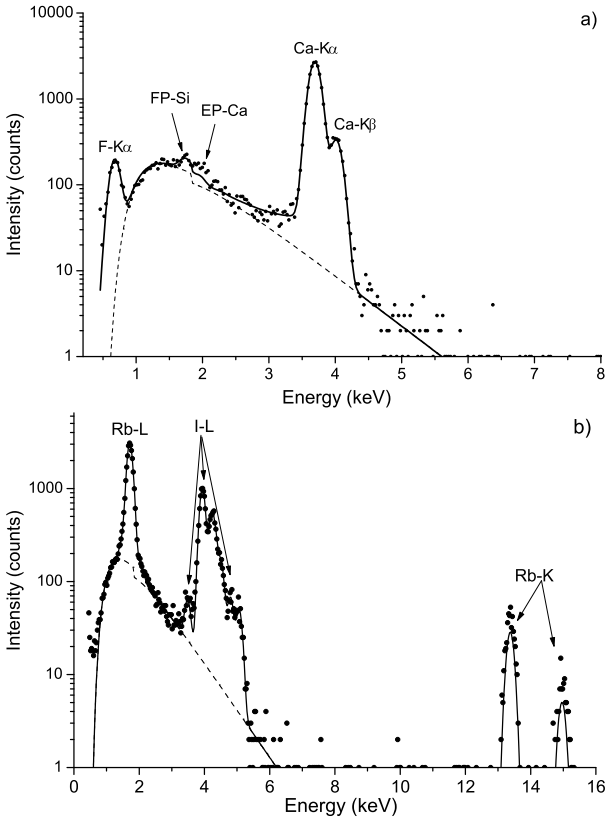

Fig. 3 Experimental (dots) and fitted (solid black line) spectrum for (a) CaF2 and (b) RbI. The fitted background is also shown (dashed line). "FP-Si" denotes the silicon internal fluorescence peak, and "EP", the escape peak.

4.2 Thick samples

For these samples, mass concentrations of 70 elements corresponding to 9 different samples detailed in Sec. 2 were determined. Tables 4 and 5 present the results obtained with PAMPA, and they are also compared with nominal concentrations and with the quantifications performed using GUPIX. From the 70 cases studied, the values obtained with PAMPA are closer to the

View Article Online
DOI: 10.1039/C7JA00068E

nominal concentrations for 33 elements, while GUPIX produced closer concentrations in 29 cases. For the remainder 8 elements, both programs produced indistinguishable results. On the other hand, if the global parameter ϵ is analized, PAMPA gave better results in 4 samples and GUPIX produced better analysis for 5 samples. In addition, special attention was paid to low concentration elements. If only the 30 analytes in concentrations lower than 1% are considered, PAMPA produced better results than GUPIX in 14 cases; GUPIX gave better values than PAMPA for 8 analytes, and in the remainder 8 cases the same results were obtained with both programs.

The relative differences of concentrations obtained with PAMPA and GUPIX with respect to the nominal values, $\Delta C/C$, are shown in the histograms of Fig. 5. It can be seen that both histograms have a similar shape.

4.3 Error estimation

The program PAMPA estimates the uncertainties in the obtained concentrations by propagating the errors associated with counting statistics, given by the square root of the number of counts, through the function I_i that describes the X-ray spectrum. A more detailed explanation of this subject is given in a previous publication about a similar software designed for electron probe microanalysis which uses the same routine for error estimation[45]. The algorithm of error propagation, roughly assumes that the analytical models used are free of error. To take these sources of error into account, the relative error determined by the program should be summed in quadrature with the relative uncertainty estimated for the detector efficiency and for certain atomic parameters.

It is difficult to give a realistic estimation of the uncertainties associated with the detector efficiency. The method implemented by Limandri *et al.*[33] to obtain the efficiency used here involves the determination of x-ray yields, which in turn, depend on several atomic magnitudes (*e. g.* ionization cross sections, fluorescence yields and relative transition probabilities) that are also included in the quantification procedure. A conventional error propagation of these magnitudes would consider three times their errors: two times for the x-ray yield ratio necessary to obtain the efficiency, and an additional contribution related to the quantification itself. This error estimation would lead to unrealistically large values, because eventual error cancellations would not be taken into account.

Regarding the errors in the atomic parameters, the most influential ones for the K shell are three: 1. X-ray production cross sections (involving ionization cross sections and fluorescence yields), which for 2 MeV protons contribute with around 15% for O, 5% for $11 \leq Z \leq 15$, 3% for S, and 1% for $19 \leq Z \leq 27$, according to Paul and Sacher[46]; 2. Stopping power, whose uncertainty is about 3%[31] and 3. Relative transition probabilities, with errors ranging from 1% for $8 \leq Z \leq 20$[31] and 2% for $22 \leq Z \leq 27$[47].

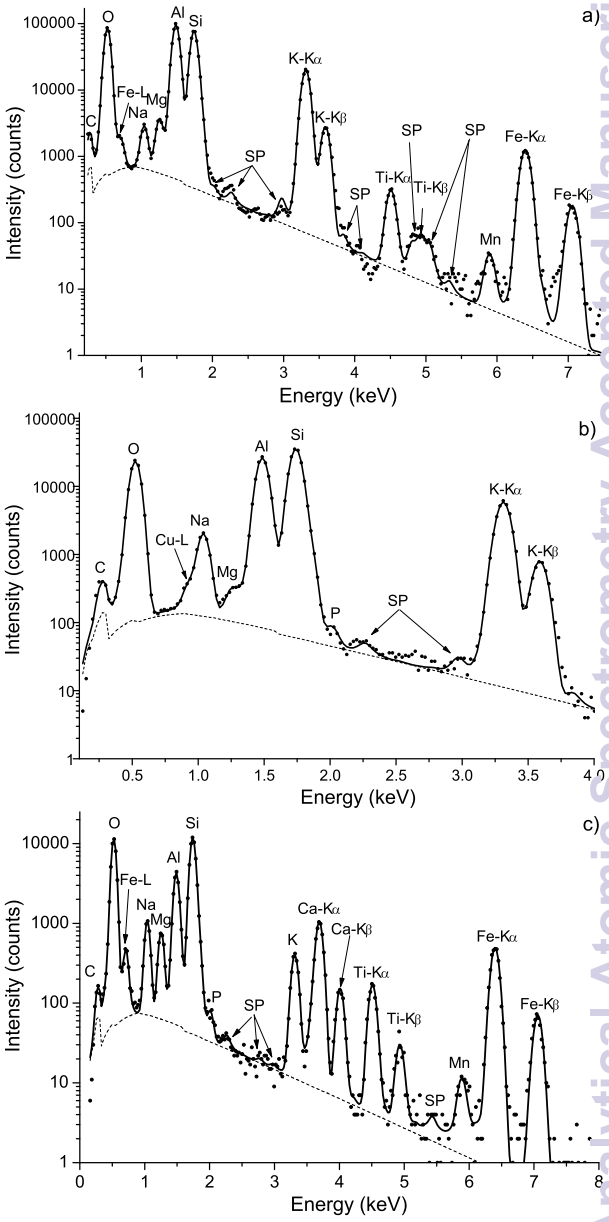

Fig. 4 Experimental (dots) and fitted (solid black line) spectrum for (a) muscovite, (b) feldspar, and c) BCR. The fitted background is also shown (dashed line). "SP" denotes sum peaks.

View Article Online
DOI: 10.1039/C7JA00068E

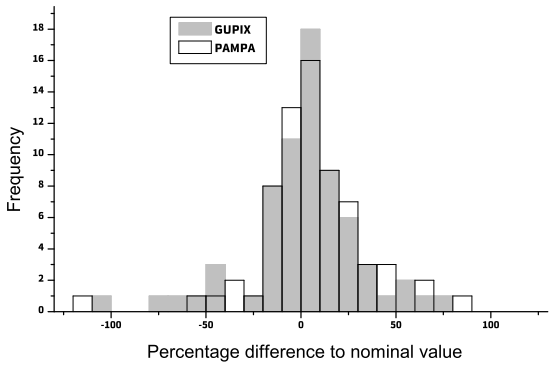

Fig. 5 Histograms of the differences of concentrations relative to the nominal values obtained by means of PAMPA (black hollow bars) and GUPIX (gray full bars). Two cases below -150% were excluded for each software.

These error values are too conservative; particularly for oxygen, they would lead to uncertainties in the concentrations between 15% and 20%, depending on the errors assigned to detector efficiency.

A more reliable estimation of errors arise from considering the quantification of several different known samples. A statistical approach to the problem would jointly account for all the contributions to the final error. To this end, the relative differences of concentrations obtained with PAMPA with respect to the nominal values, $\Delta C/C$ were considered. Since the error estimated by PAMPA involves the propagation of errors associated with the experimental intensities $\bar{I}_i$, and bearing in mind that they are important only for minor and trace elements, the error sources can be groupped in two parts: on the one hand, the contributions related to $\bar{I}_i$, and on the other hand, all the other contributions. To estimate the latter, the histogram of $\Delta C/C$ for concentrations greater than 5%, in principle free of errors due to counting statistics, was taken into account. The half width of this histogram was assessed by considering the region including 66% of the values around the centroid. The obtained value was 7%, thus, the errors in the concentrations shown in Tables 4 and 5 were estimated by summing in quadrature this number with the error assessed by the software, due only to counting statistics.

The uncertainties related to the concentrations calculated for thin samples could not be estimated because the number of studied cases is not enough to perform reliable statistics.

5 Conclusion

The software package PAMPA for spectral analysis in the field of PIXE was presented. This software minimizes the quadratic differences between the experimental spectrum and an analytical function proposed to describe it. The program has different possible applications depending on the parameters to optimize (characterization of detection efficiency, determination of transition probabilities, etc.). Particularly, when the parameters to be refined are the mass concentrations, PAMPA becomes a standardless quantification tool.

The performance of this quantification method was investigated by analizing x-ray spectra induced by proton impact in 7 thin layers and 9 thick samples. Mass concentrations were determined for 14 elements in the former materials and 70 elements in the latter. The results obtained were compared with quantifications carried out with the well-known commercial GUPIX package.

The concentrations obtained with the software presented here for thin samples are closer to the nominal values for 10 elements, while GUPIX produces closer concentrations in 4 cases. Regarding thick targets, PAMPA produces a better agreement with respect to the nominal concentrations for 33 elements, while GUPIX-s performance is better in 29 cases. From this comparison it can be stated that PAMPA produces concentrations with the same level of accuracy or slightly better than GUPIX. Particularly, PAMPA achieved a better performance for trace elements.

These first results suggest that PAMPA can be considered as an alternative quantification tool. The good performance showed in its initial application encourage the authors to make some improvements in the software; for instance, it will be necessary to make an effort for optimizing the databases used, as well as the computing time needed to carry out quantification. In addition, the analysis using x-ray filters could be included soon in the software. Finally, the possibility of performing wavelength dispersive analysis implies an easy extension of the program that could lead to the analysis of structures non-resolvable by energy dispersive spectrometry, such as satellite lines. This application would also markedly improve the precission of PAMPA as a quantification tool.

Acknowledgements

This work was financially supported by the *Secretaría de Ciencia y Técnica (Universidad Nacional de Córdoba)*. The authors are also grateful to the *Centro Atómico Bariloche*, Argentina, and to the *Centro Nacional de Aceleradores*, Sevilla, Spain, where the experimental determinations were performed.

View Article Online
DOI: 10.1039/C7JA00068E

Table 4 Mass concentrations obtained for thick samples. Numbers in parentheses are the estimated uncertainties in the last digits.

Sample	Element	Nominal	GUPIX	PAMPA
Muscovite	O	0.4623	0.4530	0.461(30)
	Na	0.0050	0.0089	0.0066(5)
	Mg	0.0060	0.0069	0.0063(4)
	Al	0.1788	0.1921	0.187(10)
	Si	0.2338	0.2321	0.232(20)
	K	0.0829	0.0849	0.0836(60)
	Ti	0.0026	0.0003	0.0024(2)
	Mn	0.0005	0.0003	0.0003(1)
	Fe	0.0282	0.0216	0.0219(10)
ε			4.0	2.1
Feldspar	O	0.4788	0.4315	0.431(30)
	Na	0.0218	0.0186	0.0188(10)
	Al	0.0972	0.1580	0.155(10)
	Si	0.3001	0.3060	0.307(20)
	P	0.0003	0.0002	0.0003(1)
	K	0.1018	0.0857	0.0872(60)
ε			13.3	13.1
Kaolinite	O	0.5093	0.4969	0.498(40)
	Na	0.0005	0.0017	0.0018(1)
	Mg	0.0011	0.0031	0.0065(5)
	Al	0.1595	0.1720	0.170(10)
	Si	0.2974	0.2977	0.296(20)
	K	0.0086	0.0098	0.0095(7)
	Ca	0.0039	0.0035	0.0034(2)
	Ti	0.0038	0.0037	0.0038(3)
	Fe	0.0158	0.0118	0.0122(9)
ε			3.4	3.6
MgO	O	0.3953	0.4487	0.456(30)
	Na	0.0112	0.0031	0.0022(2)
	Mg	0.5842	0.5371	0.530(40)
	Si	0.0028	0.0058	0.0061(4)
	S	0.0010	0.0004	0.0004(1)
	Ca	0.0054	0.0050	0.0053(4)
ε			11.1	12.7
NbO_2	O	0.2563	0.2795	0.252(20)
	Nb	0.7437	0.7205	0.749(50)
ε			4.6	1.0
BCR	O	0.4514	0.4437	0.468(30)
	Na	0.0234	0.0342	0.0300(20)
	Mg	0.0216	0.0179	0.0156(10)
	Al	0.0714	0.0854	0.0829(60)
	Si	0.2532	0.2728	0.263(20)
	P	0.0015	0.0013	0.0014(2)
	K	0.0149	0.0143	0.0135(10)
	Ca	0.0509	0.0415	0.0403(30)
	Ti	0.0135	0.0107	0.0105(8)
	Mn	0.0015	0.0011	0.0009(2)
	Fe	0.0966	0.0771	0.0735(50)
ε			8.9	9.0

Table 5 Mass concentrations obtained for thick samples. Numbers in parentheses are the estimated uncertainties in the last digits.

Sample	Element	Nominal	GUPIX	PAMPA
GSP	O	0.4844	0.4723	0.480(30)
	Na	0.0206	0.0249	0.0242(20)
	Mg	0.0058	0.0069	0.0069(5)
	Al	0.0788	0.0829	0.0815(60)
	Si	0.3110	0.3213	0.317(20)
	P	0.0013	0.0011	0.0013(1)
	K	0.0448	0.0432	0.0419(30)
	Ca	0.0150	0.0139	0.0131(9)
	Ti	0.0040	0.0038	0.0035(2)
	Fe	0.0343	0.0297	0.0298(20)
ε			4.0	2.7
Fe_2O_3 99%	O	0.3095	0.2805	0.348(20)
Al_2O_3 1%	Mg	0.0016	0.0015	0.0007(1)
	Al	0.0078	0.0091	0.0078(5)
	Si	0.0093	0.0105	0.0099(7)
	S	0.0024	0.0034	0.0033(2)
	K	0.0002	0.0001	0.0001(1)
	Ca	0.0023	0.0022	0.0019(1)
	Mn	0.0016	0.0014	0.0014(1)
	Fe	0.6656	0.6914	0.627(40)
ε			5.9	8.0
CoO 5%	O	0.3106	0.3492	0.358(30)
Cr_2O_3 95%	Si	0.0006	0.0009	0.0009(1)
	S	0.0007	0.0003	0.0003(1)
	Ca	0.0004	0.0003	0.0002(1)
	V	0.0008	0.0006	0.0006(1)
	Cr	0.6379	0.6141	0.609(40)
	Fe	0.0011	0.0016	0.0008(1)
	Co	0.0479	0.0331	0.0295(20)
ε			7.9	9.6

View Article Online
DOI: 10.1039/C7JA00068E

References

1 T. Rodríguez, S. Limandri and J. Trincavelli, *Parameter Assessment Method for PIXE Analysis*, http://www.famaf.unc.edu.ar/~trincavelli/PAMPA, 2016, [Online; accessed Dec-2016].

2 R. D. Bonetto, G. E. Castellano and J. C. Trincavelli, *X-Ray Spectrom.*, 2001, **30**, 313–319.

3 C. Visñovezky, S. Limandri, M. E. Canafoglia, R. Bonetto and J. Trincavelli, *Spectrochim. Acta Part B.*, 2007, **62**, 492–498.

4 S. Limandri, J. Trincavelli, R. Bonetto and A. Carreras, *Phys. Rev. A*, 2008, **78**, 022518 1–10.

5 J. Trincavelli, G. Castellano and R. Bonetto, *Spectrochim. Acta, Part B*, 2002, **57**, 919.

6 S. Limandri, R. Bonetto, H. D. Rocco and J. Trincavelli, *Spectrochim. Acta, Part B*, 2008, **63**, 962.

7 S. Limandri, A. Carreras, R. Bonetto and J. Trincavelli, *Phys. Rev. A*, 2010, **81**, 012504 1–10.

8 S. Limandri, R. Bonetto, A. Carreras and J. Trincavelli, *Phys. Rev. A*, 2010, **82**, 032505 1–9.

9 S. Limandri, R. Bonetto, V. G. Josa, A. Carreras and J. Trincavelli, *Spectrochim. Acta, Part B*, 2012, **77**, 44.

10 J. A. Maxwell, J. L. Campbell and W. J. Teesdale, *Nucl. Instr. Meth. Phys. Res. Sect. B*, 1989, **43**, 218–230.

11 J. A. Maxwell, W. J. Teesdale and J. L. Campbell, *Nucl. Instr. Meth. Phys. Res. Sect. B*, 1995, **95**, 407–421.

12 J. L. Campbell, T. L. Hopman, J. A. Maxwell and Z. Nejedly, *Atomic data and nuclear data tables*, 2000, **95**, 115–124.

13 J. L. Campbell, N. J. Boyd, N. Grassi, P. Bonnick and J. A. Maxwell, *Nucl. Instr. Meth. Phys. Res. Sect. B*, 2009, **268**, 3356–3363.

14 C. G. Ryan, D. R. Cousens, S. H. Sie and W. L. Griffin, *Nucl. Instr. Meth. Phys. Res. Sect. B*, 1990, **49**, 271–276.

15 I. Orlic, J. Mankjanic, G. H. J. Tros and R. D. Vis, *Nucl. Instr. Meth. Phys. Res. Sect. B*, 1990, **49**, 166–172.

16 G. Szabó and I. Borbély-Kiss, *Nucl. Instr. Meth. Phys. Res. Sect. B*, 1993, **75**, 123–126.

17 A. J. Antolak and G. S. Bench, *Nucl. Instr. Meth. Phys. Res. Sect. B*, 1994, **90**, 596–601.

18 K. Sera and S. Futatsugawa, *Nucl. Instr. Meth. Phys. Res. Sect. B*, 1996, **109/110**, 99–104.

19 S. Fazinic, M. Jaksic, J. L. Campbell, P. Van Espen, M. Blaauw and I. Orlic, *Nucl. Instr. Meth. Phys. Res. Sect. B*, 2001, **183**, 439.

20 M. Blaauw, J. L. Campbell, S. Fazinic, M. Jaksic, I. Orlic and P. Van Espen, *Nucl. Instr. Meth. Phys. Res. Sect. B*, 2002, **189**, 113.

21 C. G. Ryan, E. van Achterbergh, C. J. Yeats, T. T. Win and G. Cripps, *Nucl. Instr. Meth. Phys. Res. Sect. B*, 2002, **189**, 400–407.

22 N. Birbilis, T. Cain, J. S. Laird, X. Xia, J. R. Scully and A. E. Hughes, *ECS Electrochemistry Letters*, 2005, **4**, C34–C37.

23 C. G. Ryan, 12th International Conf. on Nuclear Microprobe Technology and Applications, 2010, p. 35.

24 S. B. Younger-Mertza, J. E. Manuel, T. Reinert, S. Z. Szilasi, S. W. Hammerstedt and G. A. Glass, *Physics Procedia*, 2015, **66**, 305–320.

25 C. Michelet, P. Barberet, G. Devès, B. Bouguelmouna, S. Bourret, M.-H. Delville, Q. L. Trequesser, N. Gordillo, D. G. Beasley, A. C. Marques, R. Farau, B. R. Toko, J. Campbell, J. Maxwell, P. Moretto and H. Seznec, *Nucl. Instr. Meth. Phys. Res. Sect. B*, 2015, **348**, 92–99.

26 T. Dupuis, G. Ghene, F. Mathis, A. Marchal, M. Philippe, H.-P. Garnir and D. Strivay, *Nucl. Instr. Meth. Phys. Res. Sect. B*, 2010, **268**, 1911–1915.

27 S. Gama, M. Volfinger, C. Ramboz and O. Rouer, *Nucl. Instr. Meth. Phys. Res. Sect. B*, 2001, **181**, 150–156.

28 D. Jembrih-Simburger, C. Neelmeijer, O. Schalm, P. Fredrickx, M. Schreiner, K. D. Vis, M. Mäer, D. Schryvers and J. Caen, *J. Anal. At. Spectrom.*, 2002, **17**, 321–328.

29 I. Atomic Energy Agency, *Intercomparison of PIXE spectrometry software packages*, IAEA-TECDOC-1342, 2003.

30 J. Nelder and R. Mead, *Comput. J.*, 1965, **7**, 308.

31 S. A. E. Johansson and J. L. Campbell, *PIXE: A novel technique for elemental analysis*, John Wiley and sons, 1988.

32 P. D. Pérez, A. P. Bertol, T. P. Rodríguez, M. A. Z. Vasconcellos and J. C. Trincavelli, *Nucl. Instr. Meth. Phys. Res. Sect. B*, 2014, **318**, 2326.

33 S. Limandri, G. Bernardi and S. Suárez, *X-Ray Spectrom.*, 2013, **42**, 487.

34 M. O. Krause, *J. Phys. Chem. Ref. Data*, 1979, **8**, 307.

35 S. T. Perkins, D. E. Cullen, M. H. Chen, J. H. Hubbell, J. Rathkopf and J. H. Scofield, *Lawrence Livermore National Laboratory Report*, 1991, **UCRL-50400 30**, 1.

36 J. L. Campbell, *Atomic data and nuclear data tables*, 2003, **85**, 291–315.

37 E. J. McGuire, *Phys. Rev. A*, 1971, **3**, 587–594.

38 W. Brandt and G. Lapicki, *Phys. Rev. A*, 1981, **23**, 1717.

39 M. G. Pia, G. Weidenspointner, M. Augelli, L. Quintieri, P. Saracco, M. Sudhakar and A. Zoglauer, *IEEE Trans. Nucl. Sci.*, 2009, **56**, 3614–3649.

40 J. F. Ziegler, M. D. Ziegler and J. P. Biersack, *Nucl. Instr. Meth. Phys. Res. Sect. B*, 2010, **268**, 1818–1823.

41 K. Heinrich, 11th Intl. Congress on X-Ray Optics and Microanalysis (ICXOM-11), 1987, pp. 67–119.

42 J. A. Bearden, *Rev. Mod. Phys*, 1967, **39**, 78.

43 J. H. Scofield, *Phys. Rev. A*, 1974, **9**, 1041–1049.

View Article Online
DOI: 10.1039/C7JA00068E

44 J. L. Campbell and J. X. Wang, *Atomic data and nuclear data tables*, 1989, **43**, 281–291.

45 R. D. Bonetto, A. C. Carreras, J. C. Trincavelli and G. E. Castellano, *J. Phys. B*, 2004, **37**, 1477.

46 H. Paul and J. Sacher, *At. Data Nucl. Data Tables*, 1989, **42**, 105.

47 S. I. Salem, T. H. Falconer and R. W. Winchell, *Phys. Rev. A*, 1972, **6**, 2147.